electronics

MDPI

Article

Generation of 3-D Grid Multi-Scroll Chaotic Attractors Based on Sign Function and Sine Function

Pengfei Ding [1,2,*], Xiaoyi Feng [1,*] and Lin Fa [2]

[1] School of Electronics and Information, Northwestern Polytechnical University, Xi'an 710072, China
[2] School of Electronics and Engineering, Xi'an University of Posts and Telecommunications, Xi'an 710121, China; falin@xupt.edu.cn
* Correspondence: dpf@xupt.edu.cn (P.D.); fengxiao@nwpu.edu.cn (X.F.)

Received: 16 November 2020; Accepted: 13 December 2020; Published: 15 December 2020

Abstract: A three directional (3-D) multi-scroll chaotic attractors based on the Jerk system with nonlinearity of the sine function and sign function is introduced in this paper. The scrolls in the X-direction are generated by the sine function, which is a modified sine function (MSF). In addition, the scrolls in Y and Z directions are generated by the sign function series, which are the superposition of some sign functions with different time-shift values. In the X-direction, the scroll number is adjusted by changing the comparative voltages of the MSF, and the ones in Y and Z directions are regulated by the sign function. The basic dynamics of Lyapunov exponent spectrum, phase diagrams, bifurcation diagram and equilibrium points distribution were studied. Furthermore, the circuits of the chaotic system are designed by Multisim10, and the circuit simulation results indicate the feasibility of the proposed chaotic system for generating chaotic attractors. On the basis of the circuit simulations, the hardware circuits of the system are designed for experimental verification. The experimental results match with the circuit simulation results, this powerfully proves the correctness and feasibility of the proposed system for generating 3-D grid multi-scroll chaotic attractors.

Keywords: sign function series; modified sine function; Jerk system; chaotic attractors

1. Introduction

Chaotic system with slight changing of initial value will produce different trajectories, and the power spectrum of chaotic system state variables is similar to random signals, the chaotic system has been widely studied around the world. Owing to deep research, the chaotic system has been applied in a great variety of engineering fields, for instance, digital image watermarking [1,2], weak signal detection [3–5], image encryption [6–10], and secure communication [11–13].

In the field of chaos, designing a chaotic system with more complex dynamical behaviors is a challengeable task and sometimes the key to solve practical application problems. In general, the number of scrolls and the direction of scrolls affect the complexity of dynamic behavior of chaotic systems. Hence, many researchers have studied the multi-scroll chaotic system with different directions, and reported large amounts of that with different dynamical characteristics. According to how many directions have generated scrolls, the multi-scroll chaotic system can be divided as one-directional (1-D) [14–23], two-directional (2-D) [17,23–26], three-directional (3-D) [25–31], and so on. A 1-D multi-scroll chaotic attractors based on Chua's circuit are designed by Suykens [14]. Tang et al. [15] realized a chaotic attractor with a 1-D multi-scroll through the modified sine function, while Wang and Liu [16] used the sign function to implement the chaotic attractor with 12 scrolls. Sánchez-López [17] using staircase functions designed 1-D and 2-D chaotic attractors, Zhang and Yu [18] used triangular wave, sawtooth wave and hysteresis sequence to realize 2-D chaotic attractors, respectively. A 1-D chaotic attractor is also designed based on a saturated nonlinear function [20],

in addition, Ding et al. [22] designed a 1-D chaotic attractor by using a special form of sine function. Günay et al. [23] designed a 1-D and 2-D multi-scroll chaotic attractor via hyperbolic tangent function. Zhang and Yu [24] used time delay hysteresis and step sequence designed a 2-D chaotic attractor, and step function with saturation to generate a chaotic attractor with scrolls in the two-direction and three-direction. Multi-segment saturated nonlinear function is also designed for generating chaotic attractors [26], Lü [27,28] introduced different methods for designing chaotic attractors with scrolls in the one-direction, two-direction and three-direction by using hysteresis function and saturated function, respectively. Zhang [29] realized a 3-D chaotic attractor based on a four-dimensional autonomous system. Lü and Chen [30] introduced the theories, methods and applications for generating 3-D multi-scroll chaotic attractors, Deng and Lü [31] proposed a 3-D multi-scroll chaotic systems based on the fractional differential system. Lately, Wang et al. [32] given a 1-D multi-scroll chaotic attractor via simplified piecewise-linear Chua's diode, and the chaotic system is verified by experimental circuits. Jia et al. [33] studied a 1-D multi-scroll chaotic attractor based on Chua's circuit with a nonlinearity of logarithmic function. Echenausía-Monroy et al. [34] introduced a fractional order chaotic system, which can generate a monostable multi-scroll attractor and coexisting attractors. Wang et al. [35] designed a 2-D multi-scroll chaotic system based on the jerk model for realizing physical layer encryption.

Yu et al. [36] used a modulating sine function as the nonlinearity in a general jerk system, and given 4-scroll and 8-scroll nesting chaotic attractors. Hu et al. [37] realized 1-D multi-scroll hidden attractors by using an improved Sprott A system with a nonlinearity of a sine function. In addition, Hu et al. [38] realized a 1-D multi-scroll chaotic attractor and a multi-butterfly wing chaotic attractor in a 5-dimensional memristive system. Fan and Yao [39] found the Chua circuit with a sine function can generate an infinite-scroll chaotic attractor, and the number of scrolls generated by this system can be adjusted by using a negative feedback control. Sun et al. [40] introduced a 3-dimensional chaotic system with three sine functions and a 4-dimensional chaotic system with four sine functions can generate infinite coexisting attractors. Lai et al. [41] studied a four-dimensional system with two sine functions, and given the phase portraits of sixteen coexisting chaotic attractors. Wu et al. [42] presented a novel and simple 3-dimensional system with two sine functions that can generate abundant coexisting multiple attractors, but not a grid multi-scroll chaotic attractor. However, none of the above chaotic systems with sine functions can generate 2-D grid multi-scroll chaotic attractors, let alone 3-D multi scroll chaotic attractors. Cafagna and Grassi [43] generated a 3-D multi-scroll hyperchaotic attractor by coupling three Chua's circuits with the sin-type function as nonlinearities forming a ring, but this 9-dimensional chaotic system is much more complex due to its nine state variables. As far as we know, there is no 3-dimensional chaotic system with nonlinearity of the sine function for generating 3-D chaotic attractor, so design a sine function based 3-D grid multi-scroll chaotic attractor is a challenging task. Inspired by the work of other researchers, we proposed a novel approach for generating 3-D grid multi-scroll chaotic attractor by using the MSF and sign function series. Scroll number in the X-direction is regulated by MSF, while the scroll number in Y-direction and Z-direction are controlled by sign function series.

2. A Novel Chaotic System for Generating 3-D Multi-Scroll Chaotic Attractors

Yalçin, Lü et al. [24,25,27,44] proposed a 3-D multi-scroll chaotic attractor, where the matrix representation of the differential equation is

$$\dot{Y} = AY + B\Phi(Y) \tag{1}$$

where,

$$A = \begin{bmatrix} 0 & 1 & 0 \\ 0 & 0 & 1 \\ -a & -a & -a \end{bmatrix}, B = \begin{bmatrix} -1 & 0 & 0 \\ 0 & -1 & 0 \\ 0 & 0 & a \end{bmatrix}, \Phi = \begin{bmatrix} h_1(y) \\ h_2(z) \\ h_3(x) \end{bmatrix} \text{ and } Y = \begin{bmatrix} x \\ y \\ z \end{bmatrix}$$

In Equation (1), if matrix Φ with a different nonlinear function of $h_1(y)$, $h_2(z)$ and $h_3(x)$, different chaotic attractors can be generated by the chaotic system (1).

Based on chaotic system (1), we designed a novel chaotic system, which can generate multi-scroll in three directions, the mathematical expression of the system is:

$$\begin{cases} \dot{x} = af_1(y) \\ \dot{y} = bf_2(z) \\ \dot{z} = -cf_1(y) - df_2(z) - ef_3(x) \end{cases} \tag{2}$$

In Equation (2), a, b, c, d and e are real constants, $f_3(x)$ is a MSF. $f_1(y)$ and $f_2(z)$ are sign function series, which are the superposition of some sign functions with different time delay values. $f_1(y)$ and $f_2(z)$ have two different forms of expression and they are described as $f_1(y) \in \{f_{11}(y), f_{12}(y)\}$ and $f_2(z) \in \{f_{21}(z), f_{22}(z)\}$. $f_{11}(y)$ and $f_{21}(z)$ for generating an odd number of scrolls, and $f_{12}(y)$ and $f_{22}(z)$ for an even number of scrolls. The representatives of the nonlinear functions of $f_3(x)$, $f_{11}(y)$, $f_{12}(y)$, $f_{21}(z)$ and $f_{22}(z)$ are given by:

$$f_3(x) = \begin{cases} -\sin(2\pi px), (-n_1/p) < x < (n_2/p) \\ \sin(2\pi px), x < -n_1/p \text{ or } x \geq n_2/p \end{cases} \tag{3}$$

$$f_{11}(y) = y - B\{\sum_{k=0}^{N_{11}} sign[y + (2k+1) * B] + \sum_{k=0}^{N_{11}} sign[y - (2k+1) * B]\} \tag{4}$$

$$f_{12}(y) = y - B[-sign(y) + \sum_{k=0}^{N_{12}} sign(y + 2k * B) + \sum_{k=0}^{N_{12}} sign(y - 2k * B)] \tag{5}$$

$$f_{21}(z) = z - B\{\sum_{k=0}^{N_{21}} sign[z + (2k+1) * B] + \sum_{k=0}^{N_{21}} sign[z - (2k+1) * B]\} \tag{6}$$

$$f_{22}(y) = z - B[-sign(z) + \sum_{k=0}^{N_{22}} sign(z + 2k * B) + \sum_{k=0}^{N_{22}} sign(z - 2k * B)] \tag{7}$$

In the X-direction, the number of scrolls is related to the nonlinear function of $f_3(x)$. Since the sine function has the characteristic of periodicity, it is used as a nonlinear function in the chaotic system by some researchers. In Refs. [19,37,38,45,46], the sine function selected as Equation (8); in Ref. [14], the sine function selected as Equation (9), and the sine function selected as Equation (10) in Refs. [47,48].

$$f(x) = \sin(2\pi bx) \tag{8}$$

$$f(x) = \begin{cases} (x - 2ac)b\pi/(2a), x \geq 2ac \\ -b\sin[\pi x/(2a) + d], -2ac < x < 2ac \\ b\pi(x + 2ac)/(2a), x \leq -2ac \end{cases} \tag{9}$$

$$f(x) = \sin(x) \tag{10}$$

If the sine functions in the form of Equations (8) and (10) are used directly to the chaotic system, the number of scrolls will be varied with transient simulation time. In order to generate a constant number of scrolls by using a sine function, a state feedback controller is used [46], for the same purpose, we change the expression of the sine function as Equation (3).

In Equation (3), p is the frequency of the sine function $f_3(x)$, n_1 and n_2 control the scroll number in the negative and positive axis of the X-direction respectively, $f_3(x)$ is depicted as Figure 1.

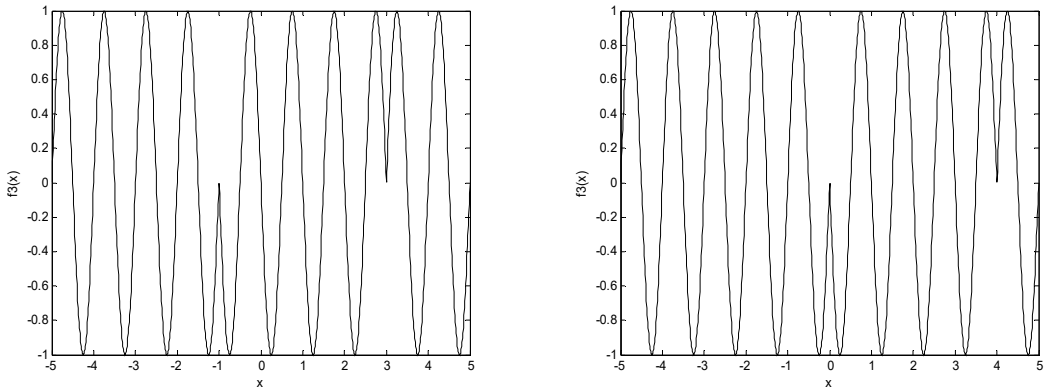

(**a**) (**b**)

Figure 1. The waveform of sine function $f_3(x)$ with $p = 1$: (**a**) $n_1 = 1$, $n_2 = 3$; (**b**) $n_1 = 0$, $n_2 = 4$.

3. Dynamics of the 3-D Multi-Scroll Chaotic Attractors

In this section, the phase portraits, Lyapunov exponents, distribution of the equilibrium point, and bifurcation diagram of the multi-scroll chaotic attractor were analyzed for understanding its dynamical behaviors.

3.1. The Phase Diagrams of the System

In Equation (2), $f_3(x)$ is selected as Equation (3), $f_1(y)$ can be selected as $f_{11}(y)$ or $f_{12}(y)$, while $f_2(z)$ can be $f_{21}(z)$ or $f_{22}(z)$, so the generated 3-D multi-scroll chaotic attractors by system (2) can be divided into four cases.

Case 1: $f_1(y) = f_{11}(y)$ and $f_2(z) = f_{21}(z)$, $(n_1 + n_2) \times (2N_{11} + 3) \times (2N_{21} + 3)$ -scrolls chaotic attractor can be generated.

Case 2: $f_1(y) = f_{12}(y)$ and $f_2(z) = f_{21}(z)$, $(n_1 + n_2) \times (2N_{12} + 2) \times (2N_{21} + 3)$ -scrolls chaotic attractor can be generated.

Case 3: $f_1(y) = f_{11}(y)$ and $f_2(z) = f_{22}(z)$, $(n_1 + n_2) \times (2N_{11} + 3) \times (2N_{22} + 2)$ -scrolls chaotic attractor can be generated.

Case 4: $f_1(y) = f_{12}(y)$ and $f_2(z) = f_{22}(z)$, $(n_1 + n_2) \times (2N_{12} + 2) \times (2N_{22} + 2)$ -scrolls chaotic attractor can be generated.

In order to illustrate the phase diagrams of the system, taking $B = 1$, $a = 1.8$, $b = 15$, $c = 6.4$, $d = 4$, $e = 4$, and the initial vales $(x_0, y_0, z_0) = (0.1, 0, 0)$ as an example, the generated multi-scroll chaotic attractors have four types.

Type 1: $n_1 = 1$, $n_2 = 2$, $f_1(y) = f_{11}(y)$, $f_2(z) = f_{21}(z)$, $N_{11} = 0$, and $N_{21} = 0$, the chaotic attractor with $3 \times 3 \times 3$-scroll is displayed in Figure 2.

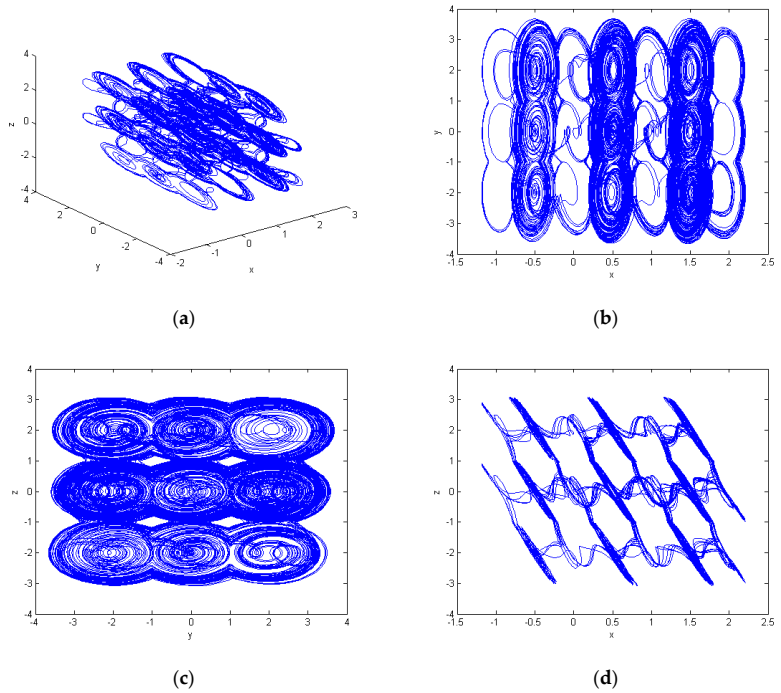

(**a**) (**b**)

(**c**) (**d**)

Figure 2. (Color online) chaotic attractors with $3 \times 3 \times 3$-scroll of system (2) with: $n_1 = 1$, $n_2 = 2$, $f_1(y) = f_{11}(y)$, $f_2(z) = f_{21}(z)$, $N_{11} = 0$, $N_{21} = 0$, and $(x_0, y_0, z_0) = (0.1, 0, 0)$: (**a**) x–y–z plane; (**b**) projection on the x–y plane; (**c**) projection on the y–z plane; and (**d**) projection on the x–z plane.

Type 2: $n_1 = 1, n_2 = 2, f_1(y) = f_{12}(y), f_2(z) = f_{21}(z), N_{12} = 1$, and $N_{21} = 0$, the chaotic attractors with $3 \times 4 \times 3$-scroll are shown in Figure 3.

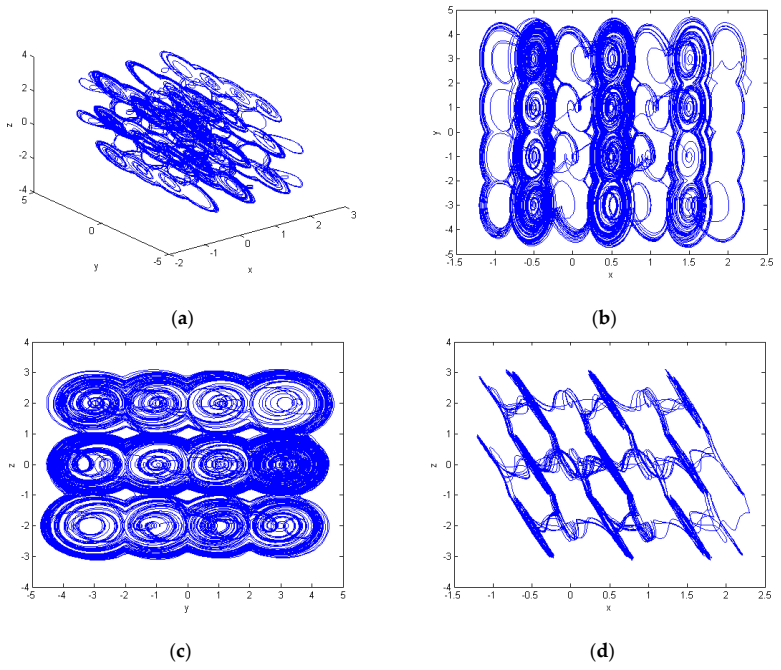

(**a**) (**b**)

(**c**) (**d**)

Figure 3. (Color online) chaotic attractor with $3 \times 4 \times 3$-scroll of system (2) with $n_1 = 1$, $n_2 = 2$, $f_1(y) = f_{12}(y)$, $f_2(z) = f_{21}(z)$, $N_{12} = 1$, $N_{21} = 0$, and $(x_0, y_0, z_0) = (0.1, 0, 0)$: (**a**) phase diagram in three-dimensional space; (**b**) projection on the x–y plane; (**c**) projection on the y–z plane; and (**d**) projection on the x–z plane.

Type 3: $n_1 = 2, n_2 = 1, f_1(y) = f_{11}(y), f_2(z) = f_{22}(z), N_{11} = 0$, and $N_{22} = 1$, the chaotic attractors with $3 \times 3 \times 4$-scroll are depicted in Figure 4.

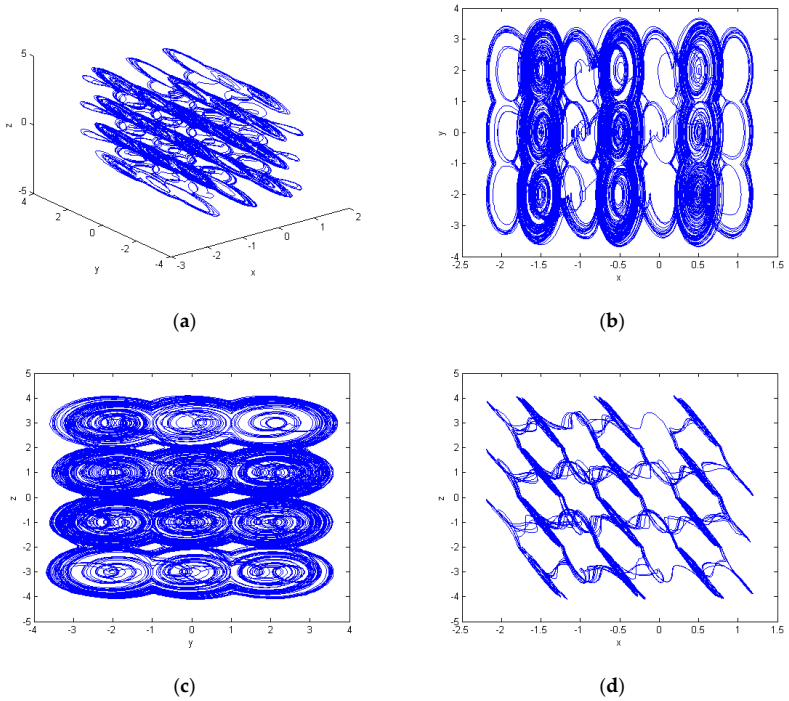

(**a**) (**b**)

(**c**) (**d**)

Figure 4. (Color online) chaotic attractor with $3 \times 4 \times 3$-scroll of system (2) with $n_1 = 2$, $n_2 = 1$, $f_1(y) = f_{11}(y)$, $f_2(z) = f_{22}(z)$, $N_{11} = 0$, $N_{22} = 1$, and $(x_0, y_0, z_0) = (0.1, 0, 0)$: (**a**) phase diagram in three-dimensional space; (**b**) projection on the x–y plane; (**c**) projection on the y–z plane; and (**d**) projection on the x–z plane.

Type 4: $n_1 = 0, n_2 = 3, f_1(y) = f_{12}(y), f_2(z) = f_{22}(z), N_{11} = 1$, and $N_{22} = 1$, the chaotic attractors with $3 \times 4 \times 4$-scroll are displayed in Figure 5.

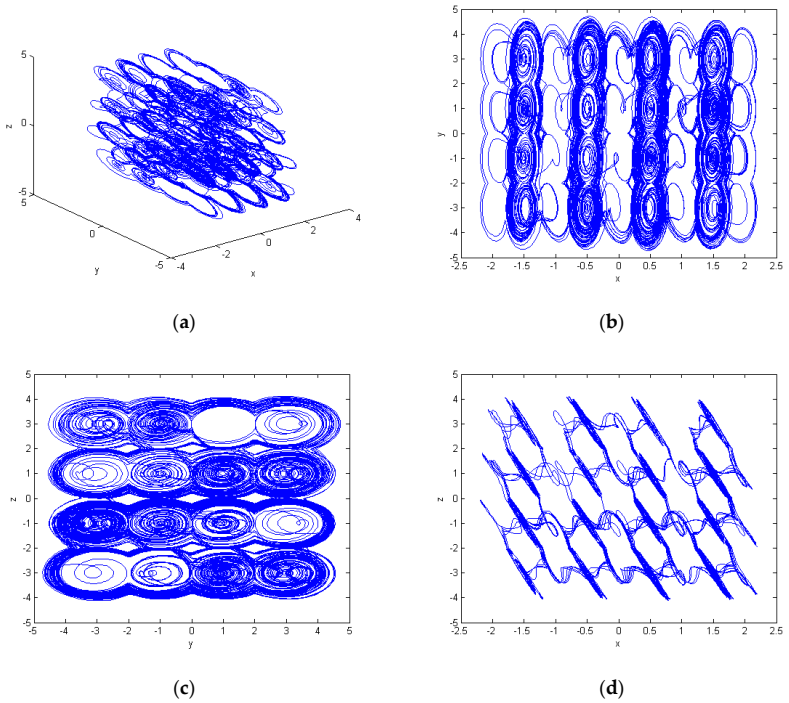

(**a**) (**b**)

(**c**) (**d**)

Figure 5. (Color online) $3 \times 4 \times 4$-scroll chaotic attractors of system (2) with $n_1 = 0$, $n_2 = 3$, $f_1(y) = f_{12}(y)$, $f_2(z) = f_{22}(z)$, $N_{11} = 1$, $N_{22} = 1$, and $(x_0, y_0, z_0) = (0.1, 0, 0)$: (**a**) x–y–z plane; (**b**) projection on the x–y plane; (**c**) projection on the y–z plane; and (**d**) projection on the x–z plane.

3.2. The Distribution of Equilibrium Points

The distribution of equilibrium points (x_e, y_e, z_e) of system (2) can be obtained by making $\dot{x} = 0, \dot{y} = 0$ and $\dot{z} = 0$.

$$\begin{cases} af_1(y) = 0 \\ bf_2(z) = 0 \\ cf_1(y) - df_2(z) - ef_3(x) = 0 \end{cases} \tag{11}$$

According to Equation (11), x_e is determined by $f_3(x)$, which is described as Equation (3). The solution of x_e is described as Equation (12).

$$x_e = \begin{cases} x_{e1} = 2nT_1, -n_1 < n < n_2, T_1 = 1/(2p), n \in Z \\ x_{e2} = 2(n+1)T_1, -n_1 < n < n_2, T_1 = 1/(2p), n \in Z \end{cases} \tag{12}$$

For y_e, it is determined by $f_1(y)$, which can be selected as $f_{11}(y)$ or $f_{12}(y)$, and they are described as Equations (4) and (5), respectively. Taking $f_1(y) = f_{11}(y)$, as an example, y_e is given as

$$y_e = \begin{cases} y_{e1} = 2mA, -(N_{11}+1) \le m \le N_{11}+1, m \in Z \\ y_{e2} = (2m+1)A, -N_{12} \le m \le N_{12}, m \in Z \end{cases} \tag{13}$$

Regarding z_e, it is determined by $f_2(z)$, which can be chosen as $f_{21}(z)$ or $f_{22}(z)$, and they are given as Equations (6) and (7), respectively. Taking $f_2(z) = f_{21}(z)$ as an example, z_e is given as

$$z_e = \begin{cases} z_{e1} = 2kA, -(N_{21}+1) \le k \le N_{21}+1, k \in Z \\ z_{e2} = (2k+1)A, -N_{22} \le k \le N_{22}, k \in Z \end{cases} \tag{14}$$

From Equations (12)–(14), the equilibrium points of Equation (13) have eight cases, which are $E_1 = (x_{e1}, y_{e1}, z_{e1})$, $E_2 = (x_{e1}, y_{e1}, z_{e2})$, $E_3 = (x_{e1}, y_{e2}, z_{e1})$, $E_4 = (x_{e1}, y_{e2}, z_{e2})$, $E_5 = (x_{e2}, y_{e1}, z_{e1})$, $E_6 = (x_{e2}, y_{e1}, z_{e2})$, $E_7 = (x_{e2}, y_{e2}, z_{e1})$, and $E_8 = (x_{e2}, y_{e2}, z_{e2})$.

Let $B = 1$, $a = 1.8$, $b = 15$, $c = 6.4$, $d = 4$, $e = 4$, and $p = 1$, the equation expression for solving the equilibrium point at E_1 is:

$$J_1 = \begin{bmatrix} 0 & af_1'(y) & 0 \\ 0 & 0 & bf_2'(z) \\ -ef'(x) & -cf_1'(y) & -df_2'(z) \end{bmatrix} = \begin{bmatrix} 0 & a & 0 \\ 0 & 0 & b \\ 2\pi eh & -c & -d \end{bmatrix} = \begin{bmatrix} 0 & 1.8 & 0 \\ 0 & 0 & 15 \\ 8\pi & -6.4 & -4 \end{bmatrix} \tag{15}$$

For Equation (15), its characteristic equation is given as follows:

$$|\lambda I - J_1| = \lambda^3 + 4\lambda^2 + 96\lambda - 216\pi = 0 \tag{16}$$

In Equation (16) I is the unit matrix, its eigenvalues are $\lambda_{11} = 4.873, \lambda_{12} = -4.437 + 10.934i, \lambda_{13} = -4.437 - 10.934i$, so equilibrium points $E_1 = (x_{e1}, y_{e1}, z_{e1})$ are saddle points of index 1. The analysis method of the rest equilibrium points is the same as that of equilibrium point E_1. The equilibrium point types are described in Table 1.

Table 1. The equilibrium point types of system (2).

Equilibrium Points	Corresponding Characteristic Root	Index Type of Saddle Point
$E_1 = (x_{e1}, y_{e1}, z_{e1})$	$\lambda_{11} = 4.873, \lambda_{12} = -4.437 + 10.934i, \lambda_{13} = -4.437 - 10.934i$	index 1
$E_2 = (x_{e1}, y_{e1}, z_{e2})$	$\lambda_{21} = 134.177,\ \lambda_{22} = 5.757,\ \lambda_{23} = -25.198$	index 2
$E_3 = (x_{e1}, y_{e2}, z_{e1})$	$\lambda_{31} = 46.350,\ \lambda_{32} = 7.286,\ \lambda_{33} = -57.636$	index 2
$E_4 = (x_{e1}, y_{e2}, z_{e2})$	$\lambda_{41} = 0.071,\ \lambda_{42} = 0.538 + 2.745i,\ \lambda_{43} = 0.538 - 2.745i$	index 2
$E_5 = (x_{e2}, y_{e1}, z_{e1})$	$\lambda_{51} = -6.193,\ \lambda_{52} = 1.096 + 10.410i,\ \lambda_{53} = 1.096 - 10.410i$	index 2
$E_6 = (x_{e2}, y_{e1}, z_{e2})$	$\lambda_{61} = 136.03,\ \lambda_{62} = -10.65 + 5.45i,\ \lambda_{63} = -10.65 - 5.45i$	index 1
$E_7 = (x_{e2}, y_{e2}, z_{e1})$	$\lambda_{71} = 53.849,\ \lambda_{72} = -7.126,\ \lambda_{73} = -50.723$	index 1
$E_8 = (x_{e2}, y_{e2}, z_{e2})$	$\lambda_{81} = -6.99,\ \lambda_{82} = 60.86 + 275.92i,\ \lambda_{83} = 60.86 - 275.92i$	index 2

From Table 1, it can be seen that there are eight kinds of equilibrium points of system (2) with $f_1(y) = f_{11}(y)$ and $f_2(z) = f_{21}(z)$, among which five cases are saddle points of index 2, and the other cases are saddle points of index 1. When $f_1(y) = f_{11}(y)$ and $f_2(z) = f_{22}(z)$, or $f_1(y) = f_{12}(y)$ and $f_2(z) = f_{21}(z)$, or $f_1(y) = f_{12}(y)$ and $f_2(z) = f_{22}(z)$, the equilibrium point types of system (2) has a similar result. Compare the result of Table 1 with Figure 2, it can be found that the generated scrolls only around the saddle points of index 2 of equilibrium points E_5. So, the equilibrium point with saddle points of index 2 is a necessary but not sufficient condition to generate the scroll.

3.3. Bifurcation Diagram and Lyapunov Exponents Spectrum

For facilitating the analysis of the Lyapunov exponents and bifurcation diagram of system (2), the parameters were selected as $f_1(y) = f_{11}(y)$ with $N_{11} = 0$, $f_2(z) = f_{21}(z)$, with $N_{21} = 0$, $f_3(x)$ with $n_1 = 1$ and $n_2 = 2$, $a = 1.8$, $b = 15$, $c = 6.4$, and $d = 4$. Varying parameter e from 3.5 to 6 with step 0.01, the Lyapunov exponent and bifurcation diagram are displayed in Figure 6a,b, respectively.

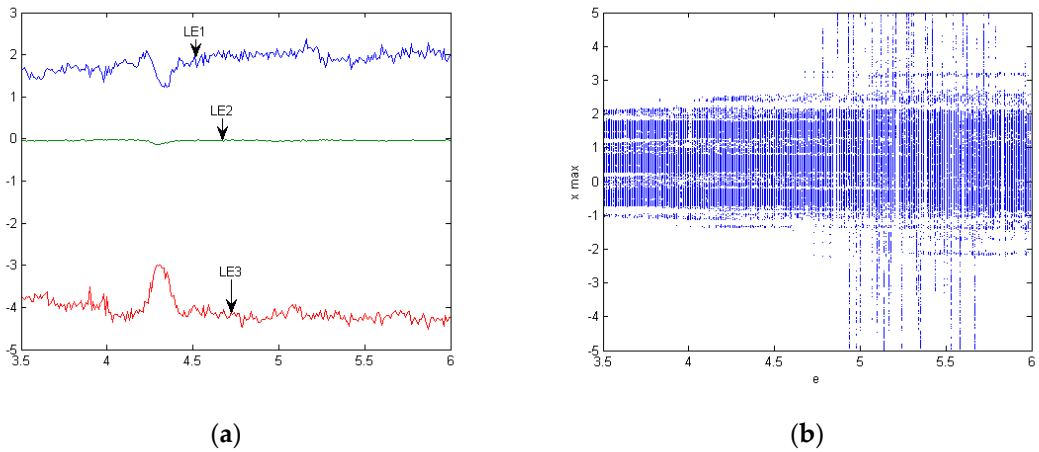

(**a**) (**b**)

Figure 6. (Color online) Bifurcation diagram and Lyapunov exponents under the conditions of $f_1(y) = f_{11}(y)$, with $N_{11} = 0$, $f_2(z) = f_{21}(z)$, with $N_{21} = 0$, $f_3(x)$ with $n_1 = 1$ and $n_2 = 2$, $a = 1.8$, $b = 15$, $c = 6.4$, $d = 4$, and $(x_0, y_0, z_0) = (0.1, 0, 0)$: (**a**) Lyapunov exponents and (**b**) bifurcation diagram.

Figure 6a,b indicates that when $e \in [3.5, 6]$, $LE1 > 0$, $LE2 = 0$, and $LE3 < 0$, the Lyapunov exponents in accordance with the bifurcation diagram. In Figure 6b, there were some values of e at the range of $e \in (4.8, 5.7)$ causing system (2) to generate more than 3-scrolls in the X-direction. For instance, system (2) with $e = 5.0$ and $(x_0, y_0, z_0) = (0.1, 0, 0)$ generated 6-scrolls in the X-direction, where the phase portraits are shown in Figure 7.

It should be noted that the system parameters in Figures 2 and 7 were identical except parameter e, the parameter e of Figure 2 was 4, while that of Figure 7 was 5. By comparing Figures 2 and 7, it can be concluded that the number of scrolls generated by system (2) in the X-direction could be determined by the parameters n_1 and n_2, while the system with suitable parameters.

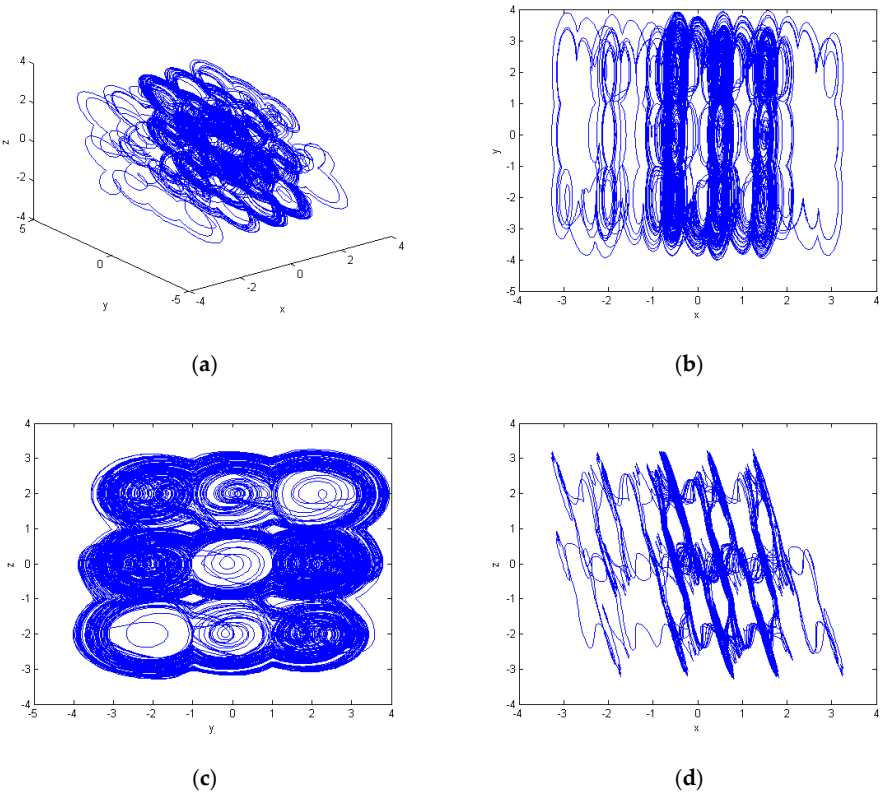

Figure 7. (Color online) $6 \times 3 \times 3$-scroll chaotic attractor of system (2) with $n_1 = 1, n_2 = 2, f_1(y) = f_{11}(y)$, $f_2(z) = f_{21}(z), N_{11} = 0, N_{21} = 0, e = 5.0$, and $(x_0, y_0, z_0) = (0.1, 0, 0)$: (**a**) x–y–z plane; (**b**) projection on the x–y plane; (**c**) projection the y–z plane; and (**d**) projection on the x–z plane.

3.4. Generation Mechanism Analysis of the Chaotic Attractors

The generation mechanism of a different number of scrolls in a certain direction is the same, so we took the chaotic attractor with a $3 \times 3 \times 3$-scroll shown in Figure 2 for analyzing the generation mechanism of this system. From Figure 2, it can be seen that when $y = z = 0$, the system generated three scrolls on the X-axis, the corresponding equilibrium points were $P_{-0.5}(-0.5, 0, 0)$, $P_0(0, 0, 0)$, $P_{0.5}(0.5, 0, 0)$, $P_1(1, 0, 0)$, and $P_{1.5}(1.5, 0, 0)$. The five equilibrium points are plotted in Figure 8.

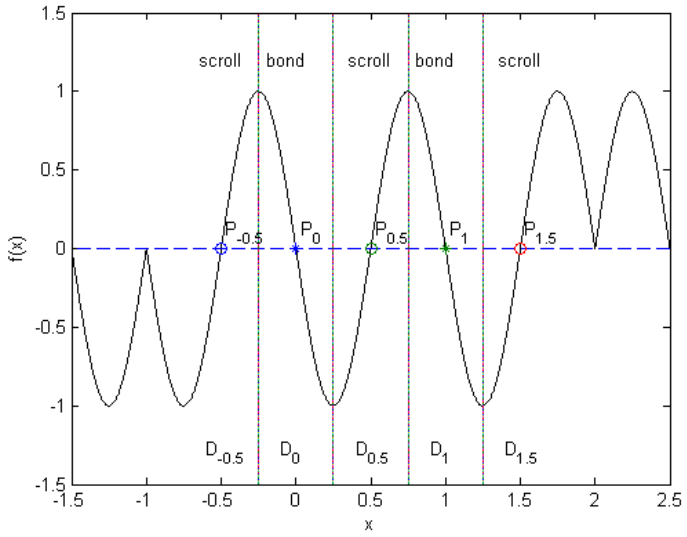

Figure 8. The equilibrium points of the $3 \times 3 \times 3$-scroll chaotic attractor and their corresponding region.

As analyzed in Section 3.2, $P_{-0.5}(-0.5,0,0)$, $P_{0.5}(0.5,0,0)$ and $P_{1.5}(1.5,0,0) \in E_5$, $P_0(0,0,0)$, and $P_1(1,0,0) \in E_1$. Thus, $P_{-0.5}(-0.5,0,0)$, $P_{0.5}(0.5,0,0)$, and $P_{1.5}(1.5,0,0)$ are saddle-focus equilibrium points with index 2, while $P_0(0,0,0)$ and $P_1(1,0,0) \in E_1$ are saddle-focus equilibrium points with index 1. The scrolls in regions $D_{-0.5}$, $D_{0.5}$, and $D_{1.5}$ were generated by X-axis shrinkage and other-axis tension. In regions D_0 and D_1, the trajectory of the chaotic attractor was stretching at the X-axis and shrinking at the Y-axis and Z-axis. As a result, $P_0(0,0,0)$ and $P_1(1,0,0)$ formed bond orbits. For the rest of the equilibrium points, the formation mechanism of the scrolls was similar to that of the above scrolls.

4. Electronic Circuit Simulation on Multisim 10

For examination of the feasibility of generating a 3-D multi-scroll chaotic attractor by this system, the electronic circuits of $f_3(x)$, $f_1(y)$, and $f_2(z)$ were designed on Multisim 10, and the electronic circuit simulations were given. On the basis of these circuits, the whole circuits of the chaotic system were proposed, and the feasibility of this chaotic system was approved by the electronic circuit simulations.

4.1. The Circuits of Nonlinear Functions of $f_3(x)$

The nonlinear function $f_3(x)$ is described as Equation (3), which can be changed as the following representation.

$$f_3(x) = -\sin(2\pi p x) H(x, v_{n1}, v_{n2}) \tag{17}$$

where,

$$H(x, v_{n1}, v_{n2}) = sign(x + v_{n1}) - sign(x - v_{n2}) - 1 \tag{18}$$

In Equation (18), $sign(x)$ is a signal function, when $x > 0$, its value is 0; when $x > 0$ and $x < 0$, the values are 1 and -1, respectively. Furthermore, v_{n1} and v_{n2} correspond to $-n_1/p$ and n_2/p in Equation (3), respectively. According to circuit theory, we designed the electronic circuits of Equation (18), which are shown in Figure 9a. Let $p = 1$, $n_1 = 1$, $n_2 = 2$, then $v_{b1} = -1$ V and $v_{a1} = 2$ V, the circuit simulation result of Figure 9a is shown in Figure 9b.

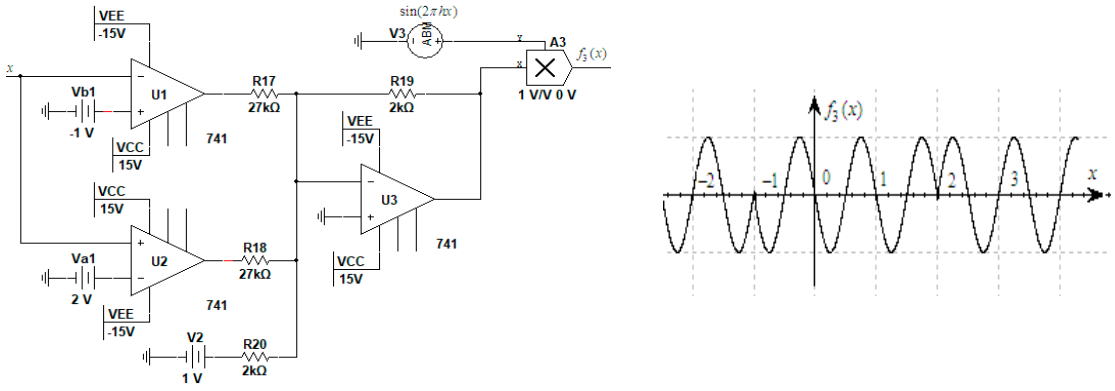

(**a**) (**b**)

Figure 9. The implement circuit of nonlinear function $f_3(x)$: (**a**) electronic circuit with $p = 1$, $n_1 = 1$ and $n_2 = 2$ and (**b**) circuit simulation result by Multisim 10.

Figures 1 and 9b show that the numerical simulation result was highly consistent with the one of electronic circuit. In implementation circuits, the change of scroll number in the X-direction only needed to modify the values of comparison voltage of v_{a1} and v_{b1} in Figure 9a.

4.2. The Circuit of Nonlinear Functions of $f_1(y)$ and $f_2(z)$

From Equations (4)–(7), it can be found that if $f_1(y)$ and $f_2(z)$ have the same expression, system (2) can generate the same number of scrolls in the Y-direction and Z-direction. Moreover, system (2) with $f_{11}(y)$ and $f_{21}(z)$ for can generate odd number of scrolls, while with $f_{12}(y)$ and $f_{22}(z)$ generate even number of scrolls. As an example, we designed the electronic circuits of $f_{11}(y)$ for generating 3-scrolls and $f_{12}(y)$ for generating 4-scrolls. The circuits and the circuit simulation results for 3-scrolls are displayed in Figure 10, while that for 4-scrolls are depicted in Figure 11.

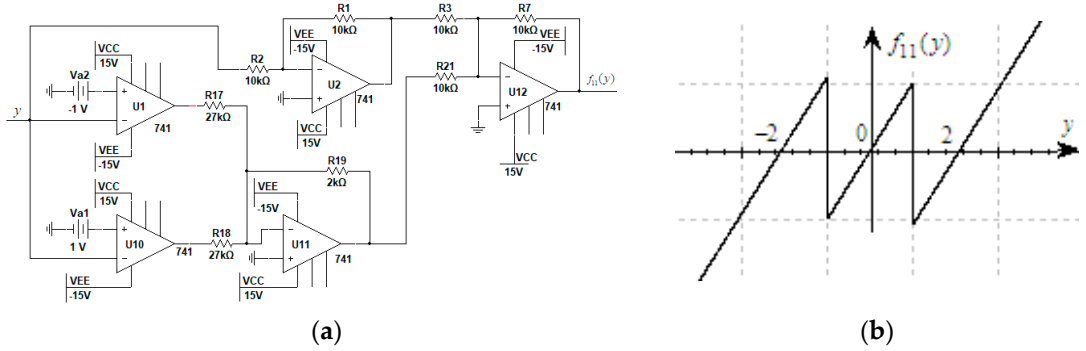

(**a**) (**b**)

Figure 10. The implement circuit of nonlinear function $f_{11}(y)$ with $N_{11} = 0$ and $B = 1$: (**a**) electronic circuit for 3-scroll and (**b**) the corresponding circuit simulation result.

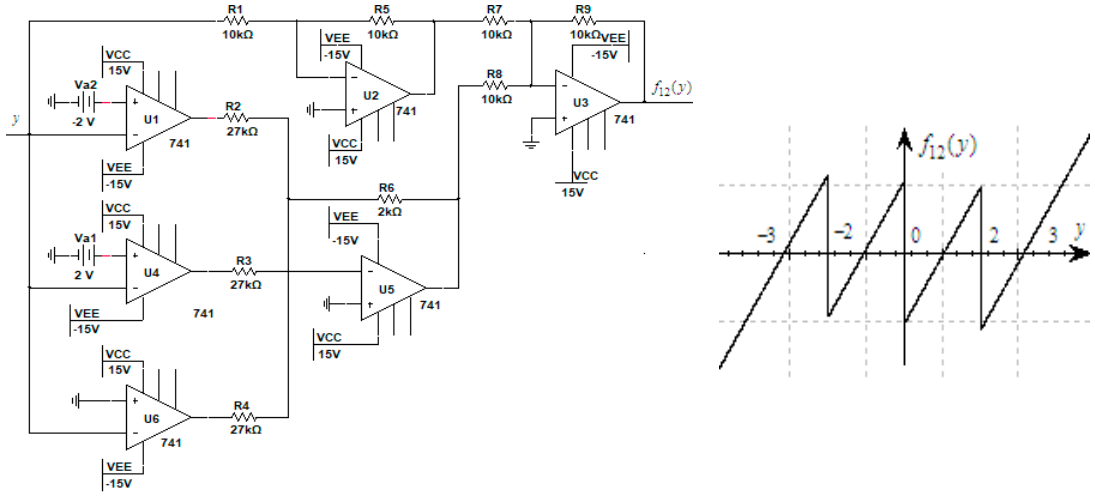

(**a**) (**b**)

Figure 11. The implement circuit of nonlinear function $f_{12}(y)$ with $N_{12} = 1$ and $B = 1$: (**a**) electronic circuit for 4-scroll and (**b**) the corresponding circuit simulation result.

In Figures 10 and 11, using z instead of the input signal y, the output signal $f_{11}(y)$ will be $f_{21}(z)$ and $f_{12}(y)$ will be $f_{22}(z)$. From Figures 10 and 11, it can be found that the circuits for generating odd and even scrolls have different circuit structures. Moreover, in Figure 10a, v_{a2}, U_1, R_{17} and v_{a1}, U_{10}, R_{18} are composed of a scroll generating circuit unit, for generating 5-scrolls in the Y-direction, a scroll generating circuit unit needs to parallel connect between the input signal y and the right of resistance R_{18}, and the two comparison voltages corresponding to v_{a1} and v_{a2} need to be set to -3 V and 3 V, respectively. Same as the circuit for generating odd number of scrolls, an additional scroll generating circuit unit is required for every additional 2-scrolls in the circuit of generating even number scrolls, and the comparison voltage of the operational amplifier in the circuit unit needs to be changed.

4.3. The Circuits of the System

Combine the circuits of $f_1(y)$, $f_2(z)$, and $f_3(x)$, the whole circuit diagram of system (2) is designed, which is shown in Figure 12. For generating odd number of scrolls in the Y-direction, $f_1(y)$ should be connected to $f_{11}(y)$, and the scroll generating circuit unit should be adjusted according to the scroll number. For generating even number of scrolls in the Y-direction, $f_1(y)$ should be connected to $f_{12}(y)$, and the scroll generating circuit unit also should be adjusted according to the scroll number. In the Z-direction, $f_2(z)$ should be connected to $f_{21}(z)$ or $f_{22}(z)$ according to the scroll number in the Z-direction.

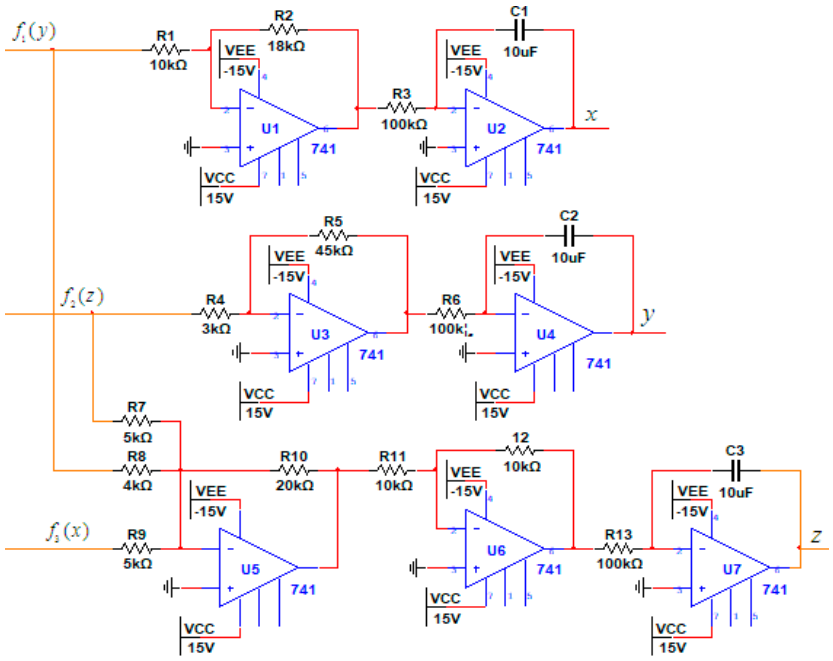

Figure 12. The implement circuit of system (2).

For the sake of examining the feasibility of circuit implementation of system (2), we made the circuit equation of Figure 12 consistent with the corresponding equations and parameters of Figures 2–5 by modifying the circuit parameters and circuit structure of Figure 12. The corresponding circuit simulation results of Figures 2–5 are shown in Figure 13, in which the unit of vertical coordinates of all graphs was 2 V/div, and the unit of horizontal coordinates of Figure 13a,c,e,g were 1 V/div, while that of the others were 2 V/div.

From the simulation results in Figures 2–5 and 13, it can be seen that the trajectory of state variables in the circuits in agreement with that of numerical simulation. The comparative voltages of v_{a1} and v_{b1} in Figure 9a determine the number of scrolls on the positive and negative part in the X-direction, respectively. The scroll numbers in the Y-direction and Z-direction were restricted by the number of scrolls generating circuit units and the structure of implementation circuits of the nonlinear functions in the Y-direction and Z-direction.

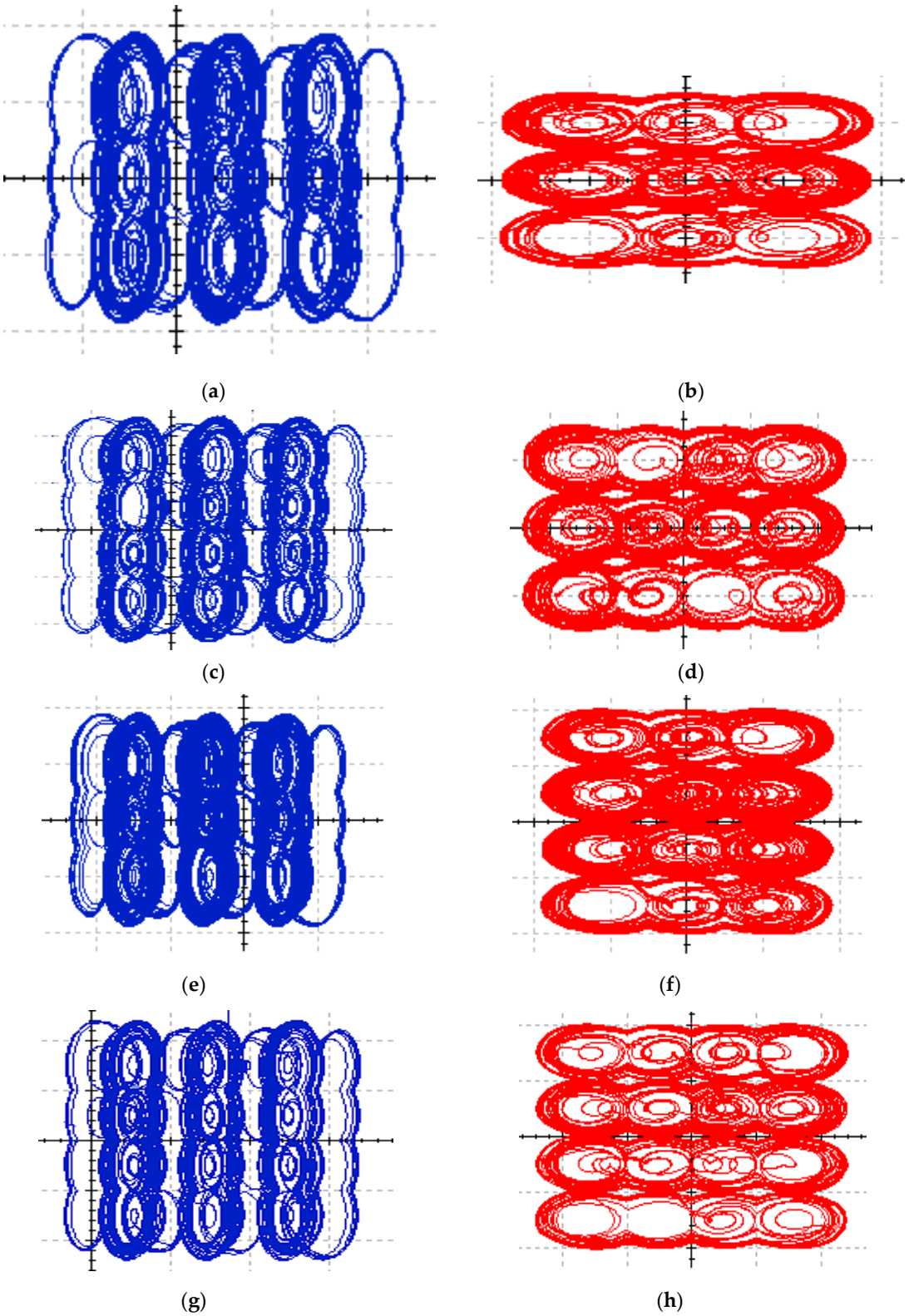

Figure 13. (Color online) The circuit simulation results correspond to Figures 5–8, respectively: (**a**,**c**,**e**,**g**) are the x–y plane and (**b**,**d**,**f**,**h**) are the y–z plane.

4.4. The Experimental Verification of the System

The circuits of the nonlinear functions of $f_3(x)$, $f_1(y)$, and $f_2(z)$ are displayed in Figures 9–11, respectively. In addition, the whole circuits of the proposed system, which are depicted in Figure 12, the hardware circuits were designed and implemented. The selection of electronic components was consistent with that of Figures 9–12. The test system for experimental verification and the experimental observations are shown in Figure 14.

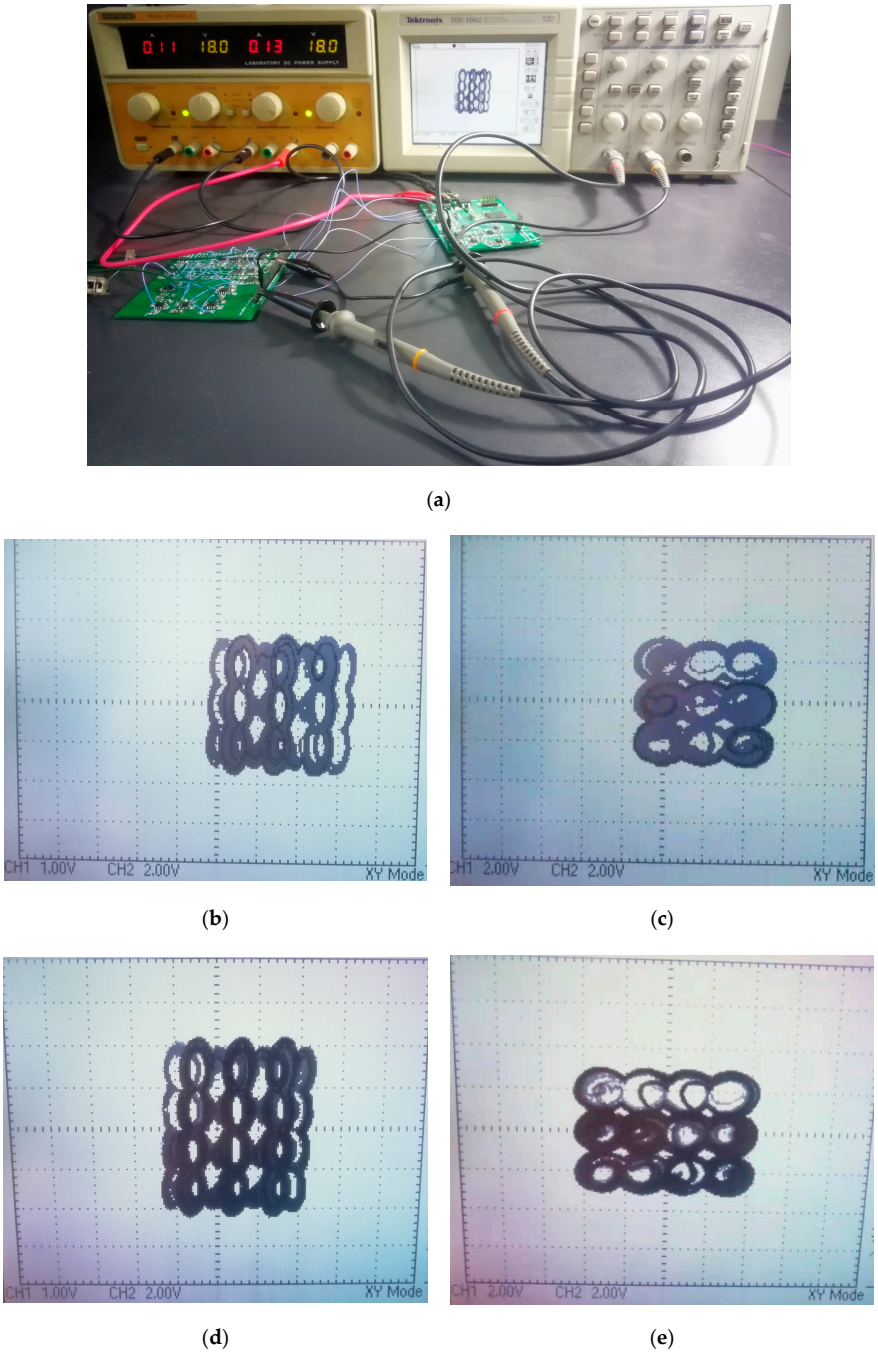

(**a**)

(**b**) (**c**)

(**d**) (**e**)

Figure 14. (Color online) The experimental verification of the proposed system: (**a**) the test system; (**b**) the experimental result of the 3 × 3 × 3-scroll in the x–y plane; (**c**) the experimental result of the 3 × 3 × 3-scroll in the y–z plane; (**d**) the experimental result of the 3 × 4 × 3-scroll in the x–y plane; and (**e**) the experimental result of the 3 × 4 × 3-scroll in the y–z plane.

As an example, we gave the experimental results of the 3 × 3 × 3-scroll and 3 × 4 × 3-scroll in the x–y plane and y–z plane. The experimental observations of Figure 14b–e corresponded to the circuit simulations of Figure 13a–d. From Figures 13 and 14, it can be seen that the hardware circuits of the proposed system could generate the same chaotic attractors generated by the circuits on Multisim 10. The experimental results indicate that the proposed chaotic system could be applied for generating 3-D multi-scroll chaotic attractors.

In the multi-scroll chaotic system, the complexity of hardware circuits was closely related to the type of nonlinear function and the structure of chaotic system. In order to compare the circuit simplicity of this system with other 3-D multi-scroll chaotic systems with circuit design and experimental results, the number of the used electronic components in circuit realization is presented in Table 2. In Table 2, [27]-1 and [27]-2 represent the 3-D multi-scroll chaotic system with nonlinearity of the hysteresis function and saturated function, respectively. n, m, and p represent the number of scrolls in the X-direction, Y-direction, and Z-direction, respectively. N_A, N_C, N_R, and N_V represent the number of used electronic components of amplifier, comparator, resistor, and reference voltage.

Table 2. Comparison of circuit realization of different 3-D multi-scroll chaotic systems.

Refs	Attractor Type	N_A	N_C	N_R	N_V
[27]-1	(2n) × (2m) × (2p) (2n + 1) × (2m + 1) × (2p + 1)	6(n + m) + 4p − 6 6(n + m) + 4p + 9	0 0	10(n + m) + 8p −1 10(n + m) + 8p + 13	2(n + m + p) − 3 2(n + m + p)
[27]-2	(2n) × (2m) × (2p) (2n + 1) × (2m + 1) × (2p + 1)	2(n + m + p) − 1 2(n + m + p) + 2	0 0	6n + 8(m + p) − 9 6n + 8(m + p) + 2	2(n + m + p) − 3 2(n + m + p) + 2
[44]	(2n) × (2m) × (2p) (2n + 1) × (2m + 1) × (2p + 1)	5 5	2n + 2m + 2p − 3 2n + 2m + 2p + 4	2n + 2m + 2p + 1 2n + 2m + 2p + 4	2n + 2m + 2p − 3 2n + 2m + 2p + 4
[49]	(2n) × (2m) × (2p) (2n + 1) × (2m + 1) × (2p + 1)	2(n + m + p) + 10 2(n + m + p) + 13	0 0	2(n + m + p) + 22 2(n + m + p) + 25	2(n + m + p) − 3 2(n + m + p)
[50]	(2n) × (2m) × (2p) (2n + 1) × (2m + 1) × (2p + 1)	2(n + m + p) + 1 2(n + m + p) + 4	0 0	6(n + m + p) − 2 6(n + m + p) + 7	2(n + m + p) − 3 2(n + m + p)
[51]	(2n) × (2m) × (2p) (2n + 1) × (2m + 1) × (2p + 1)	2(n + m + p) + 6 2(n + m + p) + 9	0 0	2(n + m + p) + 15 2(n + m + p) + 18	2(n + m + p) − 3 2(n + m + p)
This work	(2n) × (2m) × (2p) (2n + 1) × (2m + 1) × (2p + 1)	2(m + p) + 14 2(m + p) + 16	0 0	2(m + p) + 27 2(m + p) + 29	2(m + p) 2(m + p) + 2

From Table 2, it can be seen that the number of used electronic components was not related to the number of scrolls generated in the X-direction, and the used electronic components were least among the 3-D multi-scroll chaotic system in the literature. As a result, the complexity of the hardware circuit was reduced, and it is beneficial to the chip integration of the system. Furthermore, the number of scrolls in X-direction is adjusted only by changing the two reference voltages, while the other 3-D multi-scroll chaotic system need to change the electronic circuit structure. Thus, this system is very convenient to change the number of scrolls in the X-direction.

4.5. Design Guidelines of the 3-D Grid Multi-Scroll Chaotic Attractors

As the above analysis, the proposed system with nonlinear functions of $f_1(y)$, $f_2(z)$, and $f_3(x)$ could generate n × m × p-scroll chaotic attractors. The n-scroll attractor in the X-direction is regulated by the modified sine function of $f_3(x)$, while the m-scroll attractor in Y-direction and the p-scroll attractor in Z-direction are adjusted by $f_1(y)$ and $f_2(z)$, respectively. In the X-direction, parameter n_1 and n_2 control the number of scrolls in negative part and positive part. In particular:

(a1) if $n_1 + n_2$ is odd, the number of scrolls in the X-direction is odd.
(a2) if $n_1 + n_2$ is even, the scroll number in the X-direction is even.

For the Y-direction, the expression of $f_1(y)$ determines whether the number of scrolls is odd or even. In fact, $f_1(y)$ has different equation expression for generating odd or even number of scrolls.

(b1) if $f_1(y) = f_{11}(y)$, the chaotic system can generate odd number of scrolls in the Y-direction.
(b2) if $f_1(y) = f_{12}(y)$, even number of scrolls can be generated in the Y-direction.

In the Z-direction, the scroll number is determined by $f_2(z)$, and $f_2(z)$ has two kinds of expressions, one for an even number of scrolls and another for an odd number of scrolls.

(c1) if $f_2(z) = f_{21}(z)$, the scroll number generated in the Z-direction is odd.
(c2) if $f_2(z) = f_{22}(z)$, the scroll number generated in the Z-direction is even.

For generating different number of scrolls in the X-direction, Y-direction, and Z-direction, one can realize it by adjusting the parameter n_1 and n_2, and selecting a different expression for $f_1(y)$ and $f_2(z)$.

5. Conclusions

In this paper, a three-dimensional autonomous system with the MSF and step function series was proposed. The working scheme of the system was analyzed by theoretical analysis. The feasibility of this system was verified via numerical simulation results and circuit simulation results. Some dynamical behaviors, such as bifurcation diagrams, equilibrium points, phase portraits, and Lyapunov exponents were discussed. On the basis of theoretical analysis, the implementation circuits of the system were designed by Multisim 10. Furthermore, the physical realization of this system was given for experimental verification. The circuit simulation results and experimental results were consistent with the numerical ones, which show the feasibility of the system.

For the realization circuit of the chaotic system, the number of scrolls in the X-direction was regulated by the comparative voltages in the circuit of the nonlinear function of the MSF. In the Y-direction and Z-direction, the scroll numbers were adjusted by the nonlinear function of step function series, which had two different forms of expression, one for generating an even number scrolls, and the other for odd number scrolls. For generating the 3-D chaotic attractor, this system compared with other chaotic system in literature has some advantages: (i) this system needs less electronic components to generate the same number of scrolls; (ii) a different scroll can be generated on the positive and negative part of the X-direction, which is much more different with other chaotic systems; and (iii) the circuit structure in the X-direction is not restricted by the scroll number, while that of other methods are closely related to the number of scrolls.

Author Contributions: Conceptualization, X.F. and P.D.; methodology, X.F.; software, P.D.; validation, P.D. and X.F.; formal analysis, X.F., P.D. and L.F.; writing—original draft, P.D.; writing—review and editing, X.F. and L.F. All authors have read and agreed to the published version of the manuscript.

Funding: This research received no external funding.

Acknowledgments: We would like to thank the Editorial board and the anonymous reviewers.

Conflicts of Interest: The authors declare no conflict of interest.

References

1. Wang, B.; Zou, F.; Zhang, Y. New memritive chaotic system and the application in digital watermark. *Optik* **2018**, *172*, 873–878. [CrossRef]
2. AlShoura, W.H.; Zainol, Z.; Teh, J.S.; Alawida, M. A New Chaotic Image Watermarking Scheme Based on SVD and IWT. *IEEE Access* **2020**, *8*, 43391–43406. [CrossRef]
3. Lu, C.; Wu, S.; Jiang, C.; Hu, J. Weak harmonic signal detection method in chaotic interference based on extended Kalman filter. *Digit. Commun. Netw.* **2019**, *5*, 51–55. [CrossRef]
4. Liu, J.; Lin, Z.; Wang, W. An improved Liu chaotic circuit for weak signal detection. *Eur. Phys. J. Plus* **2019**, *134*, 201. [CrossRef]
5. Zhu, Q.; Lin, F.; Li, H.; Hao, R. Human-autonomous devices for weak signal detection method based on multimedia chaos theory. *J. Ambient. Intell. Humaniz. Comput.* **2020**. [CrossRef]
6. Wang, X.; Su, Y. An Audio Encryption Algorithm Based on DNA Coding and Chaotic System. *IEEE Access* **2020**, *8*, 9260–9270. [CrossRef]
7. Moafimadani, S.S.; Chen, Y.; Tang, C. A New Algorithm for Medical Color Images Encryption Using Chaotic Systems. *Entropy* **2019**, *21*, 577. [CrossRef]

8. Xuejing, K.; Zihui, G. A new color image encryption scheme based on DNA encoding and spatiotemporal chaotic system. *Signal Process. Image Commun.* **2020**, *80*, 115670. [CrossRef]
9. Yasser, I.; Khalifa, F.; Mohamed, M.A.; Samrah, A.S. A New Image Encryption Scheme Based on Hybrid Chaotic Maps. *Complexity* **2020**, *2020*, 9597619. [CrossRef]
10. Allah, M.F.; Eid, M.M. Chaos based 3D color image encryption. *Ain Shams Eng. J.* **2020**, *11*, 67–75. [CrossRef]
11. Liu, J.; Wang, Z.; Shu, M.; Zhang, F.; Leng, S.; Sun, X. Secure Communication of Fractional Complex Chaotic Systems Based on Fractional Difference Function Synchronization. *Complexity* **2019**, *2019*, 1–10. [CrossRef]
12. Yu, F.; Zhang, Z.; Liu, L.; Shen, H.; Huang, Y.; Shi, C.; Cai, S.; Song, Y.; Du, S.; Xu, Q. Secure Communication Scheme Based on a New 5D Multistable Four-Wing Memristive Hyperchaotic System with Disturbance Inputs. *Complexity* **2020**, *2020*, 1–16. [CrossRef]
13. Chen, Y.-J.; Chou, H.-G.; Wang, W.-J.; Tsai, S.-H.; Tanaka, K.; Wang, H.O.; Wang, K.-C. A polynomial-fuzzy-model-based synchronization methodology for the multi-scroll Chen chaotic secure communication system. *Eng. Appl. Artif. Intell.* **2020**, *87*, 103251. [CrossRef]
14. Suykens, J.A.K.; Vandewalle, J. Generation of N-double scrolls (N = 1, 2, 3, 4, . . .). *IEEE Trans. Circuits Syst. I Fundam. Theor. Appl.* **1993**, *40*, 861–867. [CrossRef]
15. Tang, W.; Zhong, G.; Chen, G.; Man, K. Generation of n-scroll attractors via sine function. *IEEE Trans. Circuits Syst. I Fundam. Theor. Appl.* **2001**, *48*, 1369–1372. [CrossRef]
16. Fa-Qiang, W.; Chong-Xin, L. A new multi-scroll chaotic generator. *Chin. Phys.* **2007**, *16*, 942–945. [CrossRef]
17. Sánchez-López, C. Automatic synthesis of chaotic attractors. *Appl. Math. Comput.* **2011**, *217*, 4350–4358. [CrossRef]
18. Chao-Xia, Z.; Si-Min, Y. Design and implementation of a novel multi-scroll chaotic system. *Chin. Phys. B* **2009**, *18*, 119–129. [CrossRef]
19. Li, F.; Ma, J. Pattern Selection in Network of Coupled Multi-Scroll Attractors. *PLoS ONE* **2016**, *11*, e0154282. [CrossRef]
20. Munoz-Pacheco, J.M.; Guevara-Flores, D.K.; Félix-Beltrán, O.G.; Tlelo-Cuautle, E.; Barradas-Guevara, J.E.; Volos, C.K. Experimental Verification of Optimized Multiscroll Chaotic Oscillators Based on Irregular Saturated Functions. *Complexity* **2018**, *2018*, 3151840. [CrossRef]
21. Echenausía-Monroy, J.; García-López, J.; Jaimes-Reátegui, R.; Huerta-Cuellar, G. Electronic implementation dataset to monoparametric control the number of scrolls generated. *Data Brief* **2020**, *31*, 105992. [CrossRef] [PubMed]
22. Ding, P.; Feng, X. Generation of Multi-Scroll Chaotic Attractors from a Jerk Circuit with a Special Form of a Sine Function. *Electronics* **2020**, *9*, 842. [CrossRef]
23. Gunay, E.; Altun, K. Multi-Scroll Chaotic Attractors in SC-CNN via Hyperbolic Tangent Function. *Electronics* **2018**, *7*, 67. [CrossRef]
24. Chao-Xia, Z.; Si-Min, Y. Generation of grid multi-scroll Chua's chaotic attractors with combination of hysteresis and step series. *Acta Phys. Sin.* **2009**, *58*, 120–130.
25. Gotthans, T.; Hruboš, Z. Multi Grid Chaotic Attractors with Discrete Jumps. *J. Electr. Eng.* **2013**, *64*, 118–122. [CrossRef]
26. Pano-Azucena, A.D.; Rangel-Magdaleno, J.D.J.; Tlelo-Cuautle, E.; Quintas-Valles, A.D.J. Arduino-based chaotic secure communication system using multi-directional multi-scroll chaotic oscillators. *Nonlinear Dyn.* **2016**, *87*, 2203–2217. [CrossRef]
27. Lu, J.; Chen, G.; Yu, X.; Leung, H. Design and Analysis of Multiscroll Chaotic Attractors from Saturated Function Series. *IEEE Trans. Circuits Syst. I Regul. Pap.* **2004**, *51*, 2476–2490. [CrossRef]
28. Lü, J.; Yu, S.; Leung, H.; Chen, G. Experimental verification of multidirectional multiscroll chaotic attractors. *IEEE Trans. Circuits Syst. I Regul. Pap.* **2006**, *53*, 149–165.
29. Zhang, X.; Wang, C. A Novel Multi-Attractor Period Multi-Scroll Chaotic Integrated Circuit Based on CMOS Wide Adjustable CCCII. *IEEE Access* **2019**, *7*, 16336–16350. [CrossRef]
30. Lü, J.; Chen, G. Generating Multiscroll Chaotic Attractors: Theories, Methods and Applications. *Int. J. Bifurc. Chaos* **2006**, *16*, 775–858. [CrossRef]
31. Deng, W.H.; Lü, J.H. Design of multi-directional multi-scroll chaotic attractors based on fractional differential systems via switching control. *Chaos* **2007**, *16*, 043120. [CrossRef] [PubMed]
32. Wang, N.; Li, C.; Bao, H.; Chen, M.; Bao, B. Generating Multi-Scroll Chua's Attractors via Simplified Piecewise-Linear Chua's Diode. *IEEE Trans. Circuits Syst. I Regul. Pap.* **2019**, *66*, 4767–4779. [CrossRef]

33. Jia, M.M.; Jiang, H.G.; Li, W.J. Generation and application of novel Chua multi-scroll chaotic attractors. *Acta Phys. Sin.* **2019**, *68*, 130503.
34. Echenausía-Monroy, J.; Huerta-Cuellar, G.; Jaimes-Reátegui, R.; García-López, J.H.; Aboites, V.; Cassal-Quiroga, B.B.; Gilardi-Velázquez, H.E. Multistability Emergence through Fractional-Order-Derivatives in a PWL Multi-Scroll System. *Electronics* **2020**, *9*, 880. [CrossRef]
35. Wang, F.; Zhu, B.; Wang, K.; Zhao, M.; Zhao, L.; Yu, J. Physical Layer Encryption in DMT based on Digital Multi-Scroll Chaotic System. *IEEE Photonics Technol. Lett.* **2020**, *32*, 1303–1306. [CrossRef]
36. Yu, S.; Lü, J.; Leung, H.; Chen, G. Design and implementation of n-scroll chaotic attractors from a general jerk circuit. *IEEE Trans. Circuits Syst. I Regul. Pap.* **2005**, *52*, 1459–1476.
37. Hu, X.; Liu, C.; Liu, L.; Ni, J.; Li, S. Multi-scroll hidden attractors in improved Sprott A system. *Nonlinear Dyn.* **2016**, *86*, 1725–1734. [CrossRef]
38. Hu, X.; Liu, C.; Liu, L.; Yao, Y.; Zheng, G. Multi-scroll hidden attractors and multi-wing hidden attractors in a 5-dimensional memristive system. *Chin. Phys. B* **2017**, *26*, 110502. [CrossRef]
39. Li, F.; Yao, C. The infinite-scroll attractor and energy transition in chaotic circuit. *Nonlinear Dyn.* **2016**, *84*, 2305–2315. [CrossRef]
40. Sun, J.; Zhao, X.; Fang, J.; Wang, Y. Autonomous memristor chaotic systems of infinite chaotic attractors and circuitry realization. *Nonlinear Dyn.* **2018**, *94*, 2879–2887. [CrossRef]
41. Lai, Q.; Chen, C.-Y.; Zhao, X.-W.; Kengne, J.; Volos, C. Constructing Chaotic System with Multiple Coexisting Attractors. *IEEE Access* **2019**, *7*, 24051–24056. [CrossRef]
42. Wu, H.; Bao, H.; Xu, Q.; Chen, M. Abundant Coexisting Multiple Attractors' Behaviors in Three-Dimensional Sine Chaotic System. *Complexity* **2019**, *2019*, 3687635. [CrossRef]
43. Cafagna, D.; Grassi, G. New 3D-scroll attractors in hyperchaotic chua's circuits forming a ring. *Int. J. Bifurc. Chaos* **2003**, *13*, 2889–2903. [CrossRef]
44. Yalçin, M.E.; Suykens, J.A.K.; Vandewalle, J.; Özoğuz, S. Families of scroll grid attractors. *Int. J. Bifurc. Chaos* **2002**, *12*, 23–41. [CrossRef]
45. Yalçin, M.E. Multi-scroll and hypercube attractors from a general jerk circuit using Josephson junctions. *Chaos Solitons Fractals* **2007**, *34*, 1659–1666. [CrossRef]
46. Ma, J.; Wu, X.; Chu, R.; Zhang, L. Selection of multi-scroll attractors in Jerk circuits and their verification using Pspice. *Nonlinear Dyn.* **2014**, *76*, 1951–1962. [CrossRef]
47. Xiao-Hua, L. Circuitry implementation of a novel nonautonomous hyperchaotic Liu system based on sine input. *Chin. Phys. B* **2009**, *18*, 3304–3308. [CrossRef]
48. Hadef, S.; Boukabou, A. Control of multi-scroll Chen system. *J. Frankl. Inst.* **2014**, *351*, 2728–2741. [CrossRef]
49. Wang, C.; Luo, X.; Wan, Z. Generation and circuit implementation of multi-block multidirectional grid multi-scroll chaotic attractors. *Optik* **2014**, *125*, 6716–6721. [CrossRef]
50. Zuo, T.; Sun, K.H.; Ai, X.X.; Wang, H.H. Grid multi-scroll chaotic circuit based on the second generation current conveyers. *Acta Phys. Sin.* **2014**, *63*, 080501.
51. He, S.; Sun, K.; Wang, H.; Ai, X.; Xu, Y. Design of N-dimensional multi-scroll jerk chaotic system and its performances. *J. Appl. Anal. Comput.* **2016**, *6*, 1180–1194.